Briefings in Bioinformatics, 2025, **26(5)**, bbaf479
https://doi.org/10.1093/bib/bbaf479
Case Study

Predicting response and survival of lung adenocarcinoma under anti-programmed death-1 therapy using biological deep learning

Yuanyuan Wang[1], Liuchao Zhang[2], Hongyu Xie[3], Liuying Wang[2], Yaru Wang[2], Shuang Li[2], Jia He[2], Meng Wang[2], Xuan Zhang[2], Hesong Wang[2], Kang Li[2], Lei Cao[2,*]

[1]The College of Public Health, Shanghai University of Medicine & Health Sciences, 279 Zhouzhu Road, Pudong New Area, Shanghai 201318, China
[2]Department of Epidemiology and Biostatistics, Public Health College, Harbin Medical University, No. 157, Baojian Road, Nangang District, Harbin City, Heilongjiang Province 150081, China
[3]Clinical Research Center, Women's Hospital School of Medicine Zhejiang University, No. 1 Xueshi Rd, Hangzhou, Zhejiang 310006, China

*Corresponding author. Department of Epidemiology and Biostatistics, Public Health College, Harbin Medical University, No. 157, Baojian Road, Nangang District, Harbin City, Heilongjiang Province 150081, China. E-mail: caolei@hrbmu.edu.cn

Abstract

Although programmed death (PD)-1 inhibitors inhibitors have been clinically approved for the treatment of lung adenocarcinoma (LUAD), only a few patients benefit from anti-PD-1 therapy. We developed a semi-supervised biological sparse neural network (sBiosNet) based on transfer learning to fully utilize labeled and unlabeled patient data. The pathways from the Reactome database were used to sparse the sBiosNet and extract associated biological features by integrating patients' genomic mutations and copy number variation data. We assessed the performance of the sBiosNet against random forest and support vector machine using four cohorts and provided clear interpretations using the DeepLIFT algorithm. The sBiosNet achieved the best prediction with an area under the receiver operating characteristic curve (AUROC) of 0.888 and an area under the precision recall curve (AUPR) of 0.919 for responders versus non-responders on the validation cohort, and AUROC of 0.853 and AUPR of 0.894 on an independent external cohort. The ablation experiments demonstrated that biological sparsification and multi-omics data integration, transfer learning and semi-supervised learning all contributed to improving the sBiosNet's performance. We further confirmed that genes (such as TP53, FGF3, FGFR4, and EGFR) affected LUAD patients' response to PD-1 inhibitors by regulating pathways. Meanwhile, the Low-risk LUAD patients identified by the sBiosNet obtained significant longer overall survival and progression-free survival with anti-PD-1 therapy. In conclusion, the sBiosNet accurately predicts the response and survival of patients on anti-PD-1 therapy to reduce unnecessary treatment in non-responders.

Keywords: anti-PD-1 therapy; response identification; semi-supervised learning; biological sparse neural network; multi-omics integration

Introduction

The United States Food and Drug Administration (FDA) approved the clinical use of progressive disease (PD)–1 inhibitors for treating lung adenocarcinoma (LUAD) [1, 2]. Due to both tumor-intrinsic and tumor-extrinsic factors, including tumor heterogeneity and a complex, immunosuppressive tumor microenvironment (TME) characterized by immune cells [3–9], LUAD patients typically exhibit a poor objective response rate (ORR) to PD-1 inhibitors [10, 11]. For example, patients with LUAD have shown an ORR of only 15%–20% when treated with PD-1 inhibitors, leading to eventual tumor progression due to acquired drug resistance [12–16]. Consequently, there is an urgent need for predictive models to accurately identify LUAD patients' response and survival outcomes and select complete or partial response patients to receive anti-PD-1 therapy to maximize their benefits.

Several biomarkers are commonly used to identify responses to PD-1 inhibitors. These include the expression level of PD-L1 and tumor mutational burden (TMB) [17]. However, there are limitations associated with PD-L1 expression, such as non-standardized cutoff values, high costs, and technical challenges [18–20]. TMB, in contrast, measures the number of gene mutations in a tumor patient and has been approved by the FDA as a predictive biomarker for response to PD-1 inhibitors in all solid tumors, highlighting its potential clinical applications [21, 22]. However, Strickler *et al.* [23] suggested that TMB simply emphasizes the number of gene mutations, rather than focusing on specific mutations.

Due to these limitations, some genomic studies have suggested that genomic mutations and copy number variation (CNV) affecting specific genes and signaling pathways have the additional ability to predict the response to PD-1 inhibitors [24–27]. Zhang *et al.* [28] utilized genomic mutations and CNVs to build a supervised biological sparse neural network to accurately identify the response to anti-PD-1/PD-L1 therapy in advanced melanoma; they

Received: January 29, 2025. **Revised:** June 15, 2025. **Accepted:** August 25, 2025

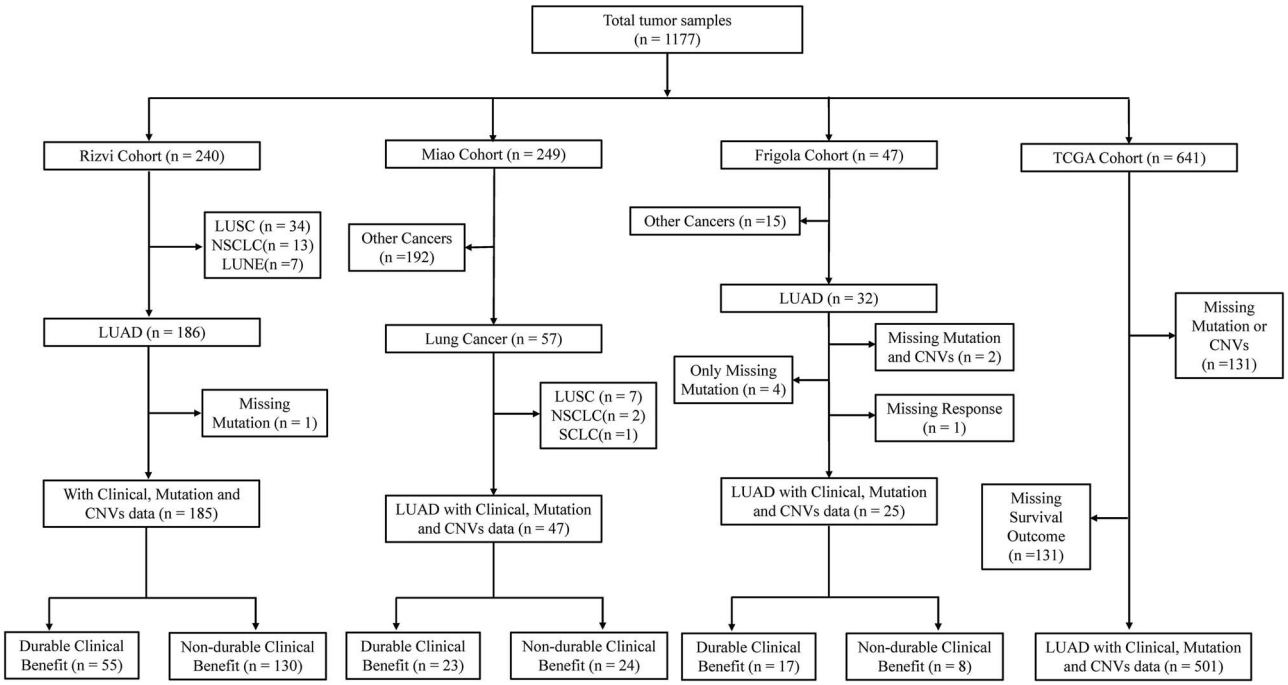

Figure 1. The process of screening samples. LUSC, lung squamous cell carcinoma; LUNE, large cell neuroendocrine carcinoma; SCLC, small cell lung cancer.

did not explore the model's ability to predict the survival outcomes of melanoma patients treated with PD-1/PD-L1 inhibitor, and its conclusions still need to be validated with a larger sample cohort. Bai *et al.* [20] developed a genomic mutation signature to predict cell lung cancer patients with a high risk of mortality after treatment with PD-1 inhibitors, but it could not accurately identify patients' objective response, which is an important criterion to demonstrate the efficacy of anti-PD-1 treatment.

Therefore, we develop a **s**emi-supervised **bio**logical **s**parse neural **net**work (sBiosNet) based on transfer learning to simultaneously identify LUAD patients' response and survival under PD-1 inhibitors treatment in by utilizing their genomic mutations and CNV profiles. The most distinct innovative aspects of sBiosNet are as follows: (i) Accurately predicting LUAD patients' response and survival under anti-PD-1 therapy using their multi-omics data and biological information from the Reactome database [29]. (ii) Improving the predictive accuracy using information from non-LUAD patients treated with PD-1 inhibitors based on semi-supervised learning and transfer learning—potentially reducing unnecessary treatment in non-responders. (iii) Provide a clear and reasonable biological process in which gene mutations and CNVs affect the response to PD-1 therapy in patients with LUAD.

Materials and methods

Clinical cohorts

There were 240 lung cancer patients molecularly profiled by MSK-IMPACT Sequencing and treated with PD-1 inhibitors in the Memorial Sloan Kettering Cancer Center dataset, and their best response to anti-PD-1 inhibitors was determined according to published response metrics by Response Evaluation Criteria in Solid Tumors (RECIST) version 1.1 [30, 31]. Gene sequencing technology and patient clinical information were described by Rizvi *et al.* [32]. We included 185 LUAD patients with genomic mutation profiles, CNV profiles, and clinical information in the Rizvi cohort, and the remaining 54 non-LUAD patients were included in the pre-training cohort (Fig. 1).

Secondly, 249 patients with cancer were profiled using whole exome sequencing [33] from the Dana-Farber Cancer Institute with anti-PD-1 therapy from Miao *et al.* [34]. We included 47 LUAD patients with genomic mutations, CNV profiles, and clinical information in the Miao cohort, and the remaining 202 non-LUAD patients were grouped into the pre-training cohort (Fig. 1). All best response of patients to PD-1 inhibitor was also assessed by RECIST v1.1.

Thirdly, 25 LUAD patients with genomic mutations, CNV profiles and best response to anti-PD-1/PD-L1 treatment from Frigola *et al.* [35] were included as an independent external validation cohort (Fig. 1).

We also selected 501 LUAD patients with genomic mutations, CNV profiles, and survival outcomes, but without anti-PD-1 therapy, from The Cancer Genome Atlas (TCGA) database as the TCGA cohort (Fig. 1). We employed TCGA cohort as a negative control to assess the ability of sBiosNet to identify survival outcomes in LUAD patients undergoing anti-PD-1 therapy.

Preprocessing of multi-omics data

In our study, genetic mutations were strictly constrained to non-synonymous mutations. In order to construct genomics mutation matrix, a value of 0 was assigned to the wild-type gene and 1 to the mutant gene, and genes with a mutation frequency of less than 1% were excluded to avoid bias. Meanwhile, we counted the total number of nonsynonymous mutations of LUAD patients and the TMB was calculated by,

$$TMB = \frac{Total\ nonsynonymous\ mutations}{Exome\ size\ \ (default: 38Mb)}$$

The TMB was reported as mutations per megabase (mutations/megabase, mut/Mb) using the R package 'maftools' [36] (version 2.8.05),

The CNV profile was annotated using R packages 'CNTools' (version 1.50.0) and categorized into amplified or deleted

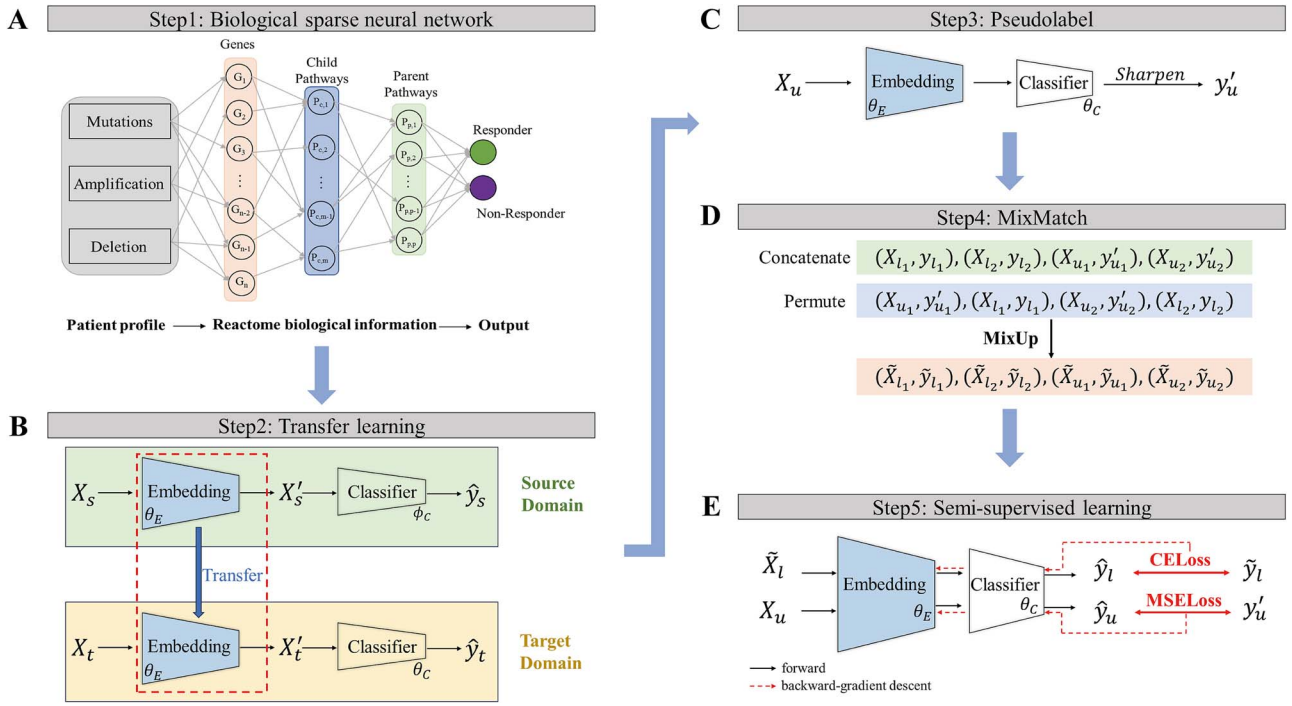

Figure 2. The flowchart of the sBiosNet. (A) Schematic diagram of biological sparse neural network. (B) The process of generating pseudo-labels. (C) Schematic diagram of the MixMatch. (D) Forward propagation process and back propagation process for semi-supervised learning.

according to the $|\ \log_2(\text{copy ratio})\ |$ exceeded 0.5. For the amplification profile, a value of 1 was assigned to the amplified gene; otherwise, a value of 0 was assigned. Similarly, in the deletion profile, a value of 1 was assigned if a gene was deleted and 0 was assigned conversely. We also excluded genes with variation rates of less than 5% in both amplification and deletion profiles.

Using genes contained in the Reactome database, 140 mutant genes, 602 amplified genes, and 13 deleted genes were filtered from all genomic mutations and CNV profiles in both the Rizvi and Miao cohorts (Supplemental Fig. S1). We found the distribution of patients between all three cohorts was no significant heterogeneity using principal component analysis (PCA) [37], t-distributed stochastic neighbor embedding (t-SNE) [38], and uniform manifold approximation and projection (UMAP) [39] (Supplemental Fig. S2).

Response stratification

According to the RECIST v1.1 [31], the duration of progression-free survival (PFS), patients achieving complete response (CR), partial response (PR), or stable disease (SD) with PFS > 6 months were classified as responders, whereas the other patients showing PD or SD with PFS ≤ 6 months were classified as non-responders [40].

The sBiosNet model

Our sBiosNet f_θ is an architecture-specific neural network constructed using the relationships of genes to child pathways and child pathways to parent pathways from the Reactome database. As shown in Fig. 2A, the sBiosNet consisted of five layers: an input layer, three hidden layers (representing the genes, child pathways, and parent pathways, respectively), and an output layer. We named the first four layers as the embedding module and the output layer as the classifier.

The number of nodes in each layer was 755, 744, 1630, 615, and 2, respectively (Supplemental Fig. S3a). Every node in the embedding module represents a biological entity such as a gene or pathway. Every edge encoded a known biological relationship between the corresponding entities, such as edge $G_1 \rightarrow P_{c,1}$ denoted by G_1 belonging to the child pathway $P_{c,1}$. Similarly, if we had known G_1 is not part of the child pathway $P_{c,2}$, then there was edge $G_1 \rightarrow P_{c,2}$ in the sBiosNet. Using such biological relationships, we could extract pathway-level features from multi-omics data of LAUD patients, which was helpful to better predict their response to PD-1 inhibitors. Meanwhile, such biological sparsification not only significantly reduced the number of parameters in sBiosNet compared with a fully connected neural network (FNN) with the same structure (Supplemental Fig. S3b), but also helped to demonstrate the contribution of these biological entities.

Such a sparse connected layer was encoded using a mask matrix A to multiply the weight matrix W to zero out all non-existing connections (Supplemental Fig. S4). Based on the input x, its output was calculated as

$$\hat{y} = (A \odot W)^T x + b$$

where b was bias vector, and $\odot$ was Hadamard product. All the mask matrix which encoded the relationships between genes and pathways used to constructed the sBiosNet were shown in Supplemental Table S1.

Each sparse layer in sBiosNet was paired with a batch normalization layer, ReLU activation function, and dropout layer. The final output layer was an FNN layer paired with a softmax function.

We first used the pre-training cohort to pre-train the embedding module in sBiosNet after the sBiosNet structure was established, and the hyperparameters used are provided in Supplemental Table S2. As shown in Fig. 2B, we used θ_E and ϕ_C to denote the parameters of the embedding module and classifier in the source domain. After the completion of pre-training, we directly used the parameters θ_E on the source domain as the initialization parameters for sBiosNet in the target domain. A pseudocode for

the sBiosNet's pre-training and training pipeline was shown in Supplemental Fig. S5 and Supplemental Fig. S6.

Semi-supervised with MixMatch

In this study, we used $L = \{(x_{l,1}, y_{l,1}), \ldots, (x_{l,n}, y_{l,n})\}$ to denote the set of LUAD patients with response labels and $U = \{(x_{u,1}), \ldots, (x_{u,m})\}$ to denote the set of unlabeled patients, where x_l and x_u are patients' multi-omics data and y_l is the response label to anti-PD-1 therapy.

For each patient, $x_u \in U$, as shown in Fig. 2C, we calculated its probability vector $\hat{y}_u = f_\theta(x_u)$ and confidence score $c_u = \max \hat{y}_u$ using sBiosNet. We then obtained its pseudo-label using the sharpened operator on $\hat{y}_u$ [41–43]:

$$y'_u = sharpen(\hat{y}_u, T) = \hat{y}_u^{\frac{1}{T}} / \sum \hat{y}_u^{\frac{1}{T}}$$

where T is a temperature parameter.

Using a threshold c_0, we classified the unlabeled patients' pseudo-labels as high confidence ($c_u > c_0$) and low confidence ($c_u \le c_0$). Thus, we further used $U_1 = \{(x_{u,1}, y'_{u,1}), \ldots, (x_{u,c}, y'_{u,c})\}$ and $U_2 = \{(x_{u,c+1}, y'_{u,c+1}), \ldots, (x_{u,m}, y'_{u,m})\}$ to denote the set of unlabeled patients with high- and low-confidence pseudo-labels.

As shown in Fig. 2D, we randomly selected (x_i, y_i) and (x_j, y_j) from the patient sets L and U_1 and generated a new 'mixed patient' using MixUp [44]. We first randomly sampled a weight λ sampled from a beta distribution with a symmetric shape parameter α. Then we re-calculate a weight $\lambda' = \max(\lambda, 1-\lambda)$ such that λ' was always greater than 0.5. Finally, we randomly mixed both patients' multi-omics data and label/pseudo-label to obtain a new 'mixed patient' $(\tilde{x}, \tilde{y})$,

$$\tilde{x} = \lambda' x_i + (1-\lambda') x_j$$

$$\tilde{y} = \lambda' y_i + (1-\lambda') y_j$$

$$\lambda' = \max(\lambda, 1-\lambda)$$

$$\lambda \sim Beta(\alpha, \alpha)$$

Due to $\lambda' > 0.5$, the first example in the MixUp operation always dominated the resulting mixed sample, which indicated $\tilde{y}$.

In our study, the semi-supervised loss consisted of a supervised cross-entropy loss between labels $\tilde{y}_l$ and model predictions $f_\theta(\tilde{x}_l)$ from the mixed labeled patient set $\tilde{L}$ and an unsupervised mean square error (MSE) between $f_\theta(x_u)$ and pseudo-labels y'_u from the unlabeled patient set U. Unsupervised loss was weighted using $w(t)$,

$$Loss = \sum_{(\tilde{x}_l, \tilde{y}_l) \sim \tilde{L}} CELoss(f_\theta(\tilde{x}_l), \tilde{y}_l) + w(t) \sum_{(x_u, y'_u) \sim U} MSELoss(f_\theta(x_u), y'_u)$$

$$w(t) = \begin{cases} 0, & if\ t \le t_0 \\ w_{max} \cdot \exp\left(-5 \times \left(\frac{t-t_0}{t_1} - 1\right)^2\right), & if\ t_0 < t < t_0 + t_1 \\ w_{max}, & if\ t \ge t_0 + t_1 \end{cases}$$

where t_0, t_1 and w_{max} were hyperparameters.

Based on the above semi-supervised loss, we updated the parameter θ in sBiosNet f_θ using gradient descent:

$$\theta_t = \theta_{t-1} - \eta \frac{\partial Loss}{\partial \theta_{t-1}}$$

where η is the learning rate.

The sBiosNet training and evaluation

In this study, the Rizvi cohort was randomly divided into an 80% training set, 10% validation set, and 10% hyperparameter selection set. The training set was used to train the pre-trained sBiosNet, and the validation and hyperparameter selection sets were used for early stopping and selecting the optimal set of hyperparameters, respectively. The Miao cohort was used as the evaluation set to assess the prediction performance of sBiosNet using the area under the receiver operating characteristic curve (AUROC), area under the precision-recall curve (AUPR), accuracy, and F1 score. We also performed 10-fold cross-validation to assess the predictive stability of sBiosNet. Moreover, the Frigola cohort was used as an independent external validation cohort to evaluate the sBiosNet's ability to identify responders to anti-PD-1/PD-L1 treatment.

During the training of the sBiosNet, we performed a grid search for the hyperparameters and the grid search ranges were shown in Supplemental Table S3. The initial learning rate of the Adam optimizer was 0.01 and decayed by $\eta_\gamma \in [0.75, 0.9]$ after every 30 epochs for a smooth convergence, and the optimizer's weight decay $w_{adam} \in [0.001, 0.0001]$). The maximum number of epochs was 400 and the epoch for early stopping was 40. The T value in the sharpened operator was 0.95, and the MixUp operator parameter $\alpha \in [0.15, 0.35]$. The confidence score threshold $c_0 \in [0.6, 0.7]$ and dropout rate for the dropout layer $p_{drop} \in [0.1, 0.2]$. In the weighting function $w(t)$, t_0 is 10, $t_1 \in [20, 30]$ and $w_{max} \in [2.5, 3.5, 4.5]$. The set of hyperparameters that maximizes the AUROC of sBiosNet on the hyperparameter selection set was chosen as the optimal hyperparameters.

We also compared sBiosNet with some models, including random forest (RF), linear support vector machine (Linear-SVM) and radial basis function-SVM (RBF-SVM), L2 logistic regression (L2-Logit), and BiosNet (a neural network similar to sBiosNet but trained with supervised learning). We searched for the optimal hyperparameters for these methods, such as the number of trees in RF ($N_{RF} \in [100, 500, 1000, 2000]$) and the regularization strength parameter in Linear-SVM, RBF-SVM, and L2-Logit ($C_{reg} \in [1.0, 2.0, 3.0, 4.0]$). The hyperparameter scope of BiosNet was the same as that of sBiosNet. As there was still no standardized cutoff value for TMB to predict response to PD-1 inhibitors in LUAD patients, we combined TMB with logistic regression analysis to explore its predictive performance.

Ablation experiments

We conducted several ablation experiments to explore the contribution of biological sparsity, multi-omics integration, semi-supervised learning, and transfer learning to sBiosNet. We built sDNet1 as an FNN with the same number of layers and nodes as sBiosNet and sDNet2 as another FNN with equivalent parametric as the sBiosNet, and its three hidden layers contained 19, 10, and 6 nodes, respectively. The neural network trained solely using CNV or genomic mutation profiles was named Only-CNV and OnlyMut. The neural network trained without transfer learning was named as no-transfer. For all ablation experiments, the hyperparameter settings were the same as those of the sBiosNet.

Biological interpretation

We used the DeepLIFT algorithms [45] a backpropagation-based attribution method, to calculate the importance score $C_{i,j}$ for the j-th node of i-th layer in the sBiosNet. To avoid nodes with more connected edges having a greater importance score, we used an

adjusted importance score $AdjC_{i,j}$ to evaluate its contribution,

$$AdjC_{i,j} = \begin{cases} \frac{C_{i,j}}{d_{i,j}}, & if\ d_{i,j} > \mu + 5\sigma \\ C_{i,j}, & if\ d_{i,j} \le \mu + 5\sigma \end{cases}$$

Where $d_{i,j}$, is the number of edges connected to the node and μ and σ are the mean and standard deviation of $d_{i,j}$ respectively.

Statistical analysis

For demographic information, the continuous variables were summarized using mean ± standard deviation and minimum-maximum, and the categorical variable were summarized using frequency and percentage. The Kruskal–Wallis rank test and χ^2 test (using the *kruskal.test* and *chisq.test* function in *stats* package, version 4.1.0) were used to compare the difference between three cohorts.

To assess the ability of sBiosNet to identify LUAD patient survival outcomes under anti-PD-1 therapy. We grouped the non-responders identified by sBiosNet into the high-risk group and responders into the low-risk group. The survival outcomes of LUAD patients between the two groups were compared using the Kaplan–Meier method and log-rank test, and hazard ratios (HR) and 95% confidence interval (95% CI) were calculated using univariate COX regression analysis. We also performed multivariate Cox regression analysis to adjust for the influence of important clinical factors (such as age, gender, smoking status). $P < .05$ was considered statistically significant.

Neural networks were implemented using PyTorch modules (version 1.7.1) in Python 3.6.8. The DeepLIFT and UMAP algorithms were performed using Captum modules (version 0.5.0) and UMAP modules (version 0.5.3), respectively. PCA, t-SNE, RF, SVM, and L2-Logit were performed using scikit-learn modules (version 0.24.2). Survival analysis and univariate Cox regression analysis were performed using the survival package (version 3.5–5) in R 4.1.0. All figures were based on the ggplot2 package (version 3.3.5), pROC package (version 1.18.0), networkD3 package (version 0.4), and survminer package (version 0.4.9). Source code is available at https://github.com/0219zhang/sBiosNet.

Result

Basic characteristics

The baseline demographic characteristics of three cohorts (Rizvi, Miao, and Frigola cohorts) were shown in Supplemental Table S4. The average age of LUAD patients in the Riavi, Miao, and Frigola cohorts was 62.24 (range: 22–92), 61.46 (range: 41–78) and 59.28 (range: 40–83) years. The distribution of gender was also almost same between all three cohorts. However, there were significant differences in the proportion of patients' smoking status among the three cohorts, with the highest proportions of current smoking in the Miao cohort at 23.4% and the lowest proportion of never smoking in the Rizvi cohort at 21.62%.

Prediction performance of the sBiosNet

Based on transfer learning, the sBiosNet learned some meaningful features that were associated with LUAD patients' response to anti-PD-1 therapy in the pre-training cohort (Supplemental Fig. S7). The optimal hyperparameters for the selected sBiosNet during the retraining process are listed in Supplemental Table S3.

Compared with RF, linear-SVM, L2-Logit, etc., sBiosNet showed the best prediction performance (AUROC = 0.888, AUPR = 0.919, Accuracy = 0.872, and F1 score = 0.864, Fig. 3A–C and Supplemental Table S5). We found that without semi-supervised learning, corresponding to the BiosNet (AUROC = 0.726), would causes a 0.162 decrease compared with the sBiosNet. Specifically, sBiosNet accurately identified 84.62% of the responders and 90.48% of the non-responders (Fig. 3D). We also found that BiosNet's AUROC was 0.726, which was significantly lower than that of sBiosNet, suggesting that semi-supervised learning was helpful in improving sBiosNet's predictive ability. Meanwhile, the combination of TMB with logistic regression (AUROC = 0.762, AUPR = 0.810) exhibited a superior ability to RF, L2-Logit, and SVMs, demonstrating the potential of TMB. However, it is important to note that we still do not know TMB's optimal cutoff value of TMB.

We further used the sBiosNet to identify the responders and non-responders from the Frigola cohort, an independent external cohort, the results showed sBiosNet still owned a satisfactory predictive performance with AUROC = 0.853, AUPR = 0.894, true negative rate (TN) = 70.00% and true positive rate = 93.33% (Fig. 4A–C).

Prediction stability of the sBiosNet

The results of 10-fold cross-validation showed that sBiosNet had the best prediction accuracy (mean AUROC = 0.868) and stability (standard deviation of AUROC = 0.027) (Supplemental Fig. S8a and Supplemental Table S6). RF and BiosNet also had better accuracy and stability than L2-Logit and SVMs, which was consistent with the results in Fig. 3. However, Rbf-SVM exhibited both lower accuracy and stability, suggesting that it was not well-suited for tasks with small sample sizes.

Similarly, the AUPR, accuracy, and F1 score exhibited the same trends as AUROC for each predictive model (Supplemental Figs. S8b–d), suggesting that sBiosNet has the advantage of identifying the response to PD-1 inhibitors in patients with LUAD. Meanwhile, the 10-fold cross-validation results on the Frigola cohort further confirmed that the sBiosNet exhibited good predictive stability, and there was no obvious overfitting of the sBiosNet in this study (Fig. 4D and Supplemental Table S7).

Ablation experiments

The ablation experiments showed that sBiosNet and sDNet2 exhibited significantly better prediction performances than sDNet1. For instance, the AUROC of sBiosNet, sDNet2, and sDNet1 were 0.888, 0.816, and 0.616, respectively (Fig. 5 and Supplemental Table S8). This result demonstrated that either dropping the nodes or edges to reduce the number of parameters in sBiosNet could improve its predictive ability. Furthermore, the higher AUROC value of sBiosNet compared to that of sDNet2 indicated that incorporating biological knowledge from the Reactome database was also beneficial.

We also found that the AUROC of the OnlyCNV and the OnlyMut were 0.646 and 0.757, respectively (Fig. 5 and Supplemental Table S8), both were inferior than the sBiosNet, suggesting integrating multi-omics data allowed the sBiosNet to capture a more comprehensive and diverse features to identify LUAD patients' response to anti-PD-1 therapy. Meanwhile, the OnlyMut AUROC was higher than that of OnlyCNV, indicating that the genomic mutation profile was more informative than the CNVs profile alone. In addition, the AUROC of the No-transfer model was only 0.661, suggesting that transfer learning contributed to improving the sBiosNet's AUROC by 0.227. Compared with the sDNet1 (AUROC = 0.616), we found the biological sparsification contributed 0.272 of AUROC to the sBiosNet.

We also performed 10-fold cross-validation based on the ablation experiments and found that sBiosNet had the largest mean

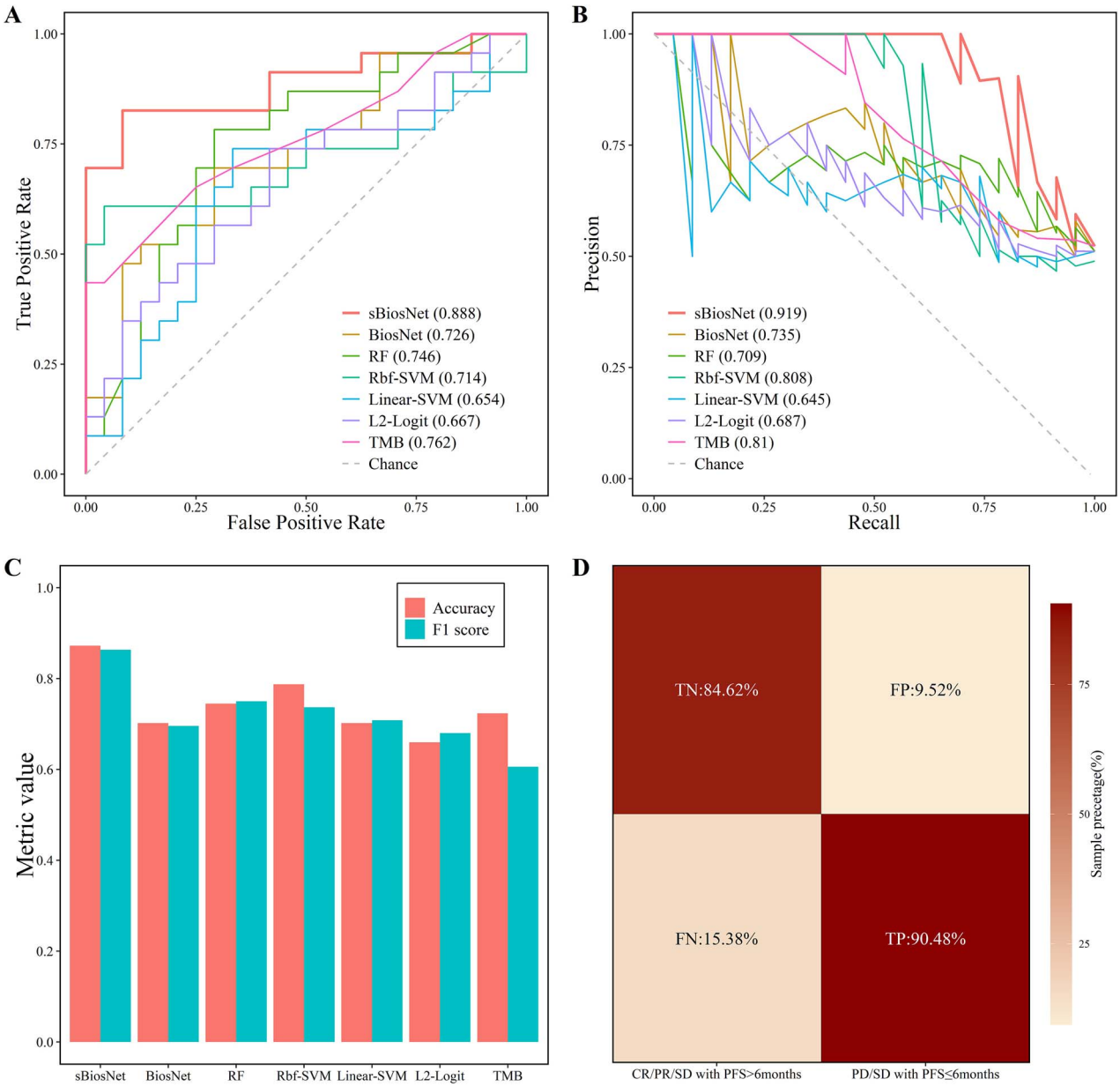

Figure 3. Performance to predict responders versus non-responders of the sBiosNet on the Miao cohort. (A) The ROC curve of seven models. (B) The PR curve of seven models. (C) The accuracy and F1 score of seven models. (D) Confusion matrix using the sBiosNet to classify the LAUD patients in Miao cohort. FP, false-positive rate; FN, false-negative rate; TP, true-positive rate.

value and the smallest standard deviation in terms of AUROC, AUPR, accuracy, and F1 score (Supplemental Fig. S9 and Supplemental Table S9). We also found that sDNet2 was superior to sDNet1 and that OnlyMut was superior to OnlyCNV. All the results are consistent with those of the ablation experiments.

Inspecting and interpreting the sBiosNet

By combining sBiosNet with the DeepLIFT algorithm, we obtained the importance score of each node in sBiosNet. We aggregated the importance scores of nodes into genomic mutation, CNV amplification, and CNV deletion in the input layer (Supplemental Table S10) and selected the top 10 nodes with the highest importance score from each hidden layer; the remaining nodes in each hidden layer were referred to as residuals (Supplemental Table S11, Supplemental Table S12, Supplemental Table S13). Based on the important score above, we visualized sBiosNet with fully interpretable layers using Sankey diagrams (Fig. 6).

Among the aggregated molecular alterations, genomic mutations were more informative than CNV amplification and deletion, which was consistent with OnlyMut being superior to OnlyCNV in the ablation experiments. Among all 744 genes, TP53 mutation had the highest importance score, and we found that this mutation functioned mainly through the Pre-NOTCH Expression and Processing pathway and the Signaling by NOTCH pathway. The genomic mutations of FGF3 and FGFR4 function first through signaling via the RTK pathway and the MAPK family signaling cascade pathway, and then through the signaling transduction pathway and EGFR signaling in the cancer pathway. Additionally, the genomic mutation and CNV amplification of EGFR also acted through the aforementioned pathways to influence the response to anti-PD-1 therapy in patients with LUAD. We also

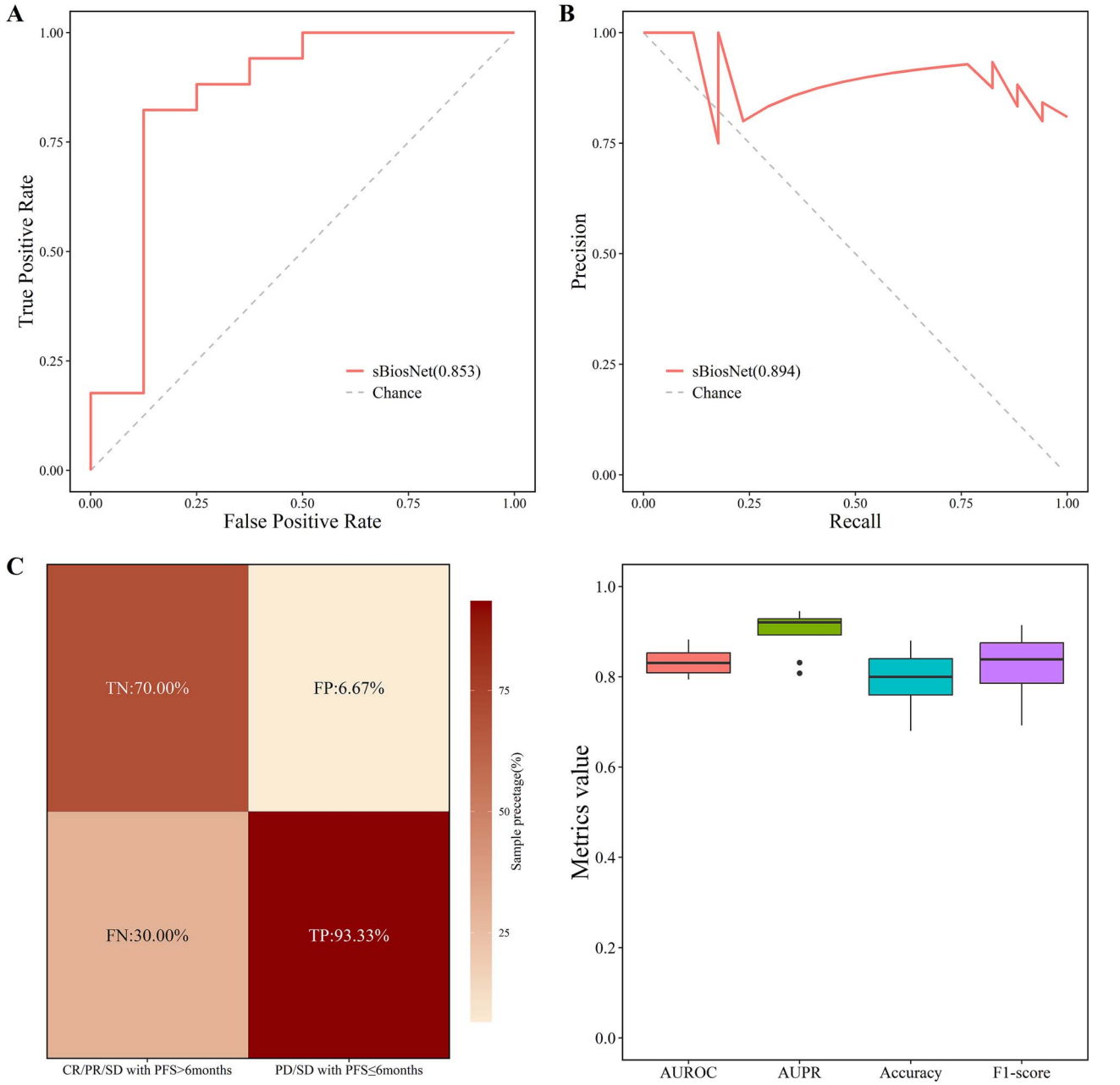

Figure 4. Prediction performance of the sBiosNet on the Frigola cohort. (A) ROC curves. (B) PR curves. (C) Confusion matrix. (D) Box plot of metrics in 10-fold cross-validation.

found that the amplification of RPA3, ST3GAL1, and RGS5 might affect the response of patients with LUAD to PD-1 inhibitors.

Validation of selected genes and pathways

We then used three independent external cohorts to validate the top 10 genes and important pathways selected by the sBiosNet and DeepLIFT algorithms. The first Hellmann cohort [46] included the genomic mutation profiles of 36 LUAD patients treated with PD-1 inhibitor. Based on their PFS and response to anti-PD-1 treatment, they were grouped into 21 responders and 15 non-responders. Using Fisher's exact test to compare the mutation frequency of the top 10 genes between the two groups, no significant association was found between these gene mutations and patient's response (Supplemental Table S14).

We also downloaded two mRNA expression profiles of non-small cell lung cancer (NSCLC) patients treated with PD-1 inhibitors (GSE202417 and GSE111414 [47]) from Gene Expression Omnibus (GEO) database for validation of those signatures at the transcriptomic level. Due to the absence of PFS for patients in these two datasets, we compared the differences in gene expression levels and gene set features between responders (CR/PR) and non-responders (SD/PD). The results showed that only the gene RGS5 in the GSE111414 was significantly downregulated in responders, while other genes were still no significant difference in the top 10 genes' expression levels between responders and non-responders (Supplemental Table S15 and Supplemental Table S16). The above results demonstrated that genomic mutations or mRNA expression of single gene was insufficient for identifying LUAD patients' response to PD-1 inhibitors.

We further used the Gene Set Enrichment Analysis (GSEA) [48, 49] to extract the gene set features for the patients in GSE202417 and GSE111414 from their mRNA expression profiles, and

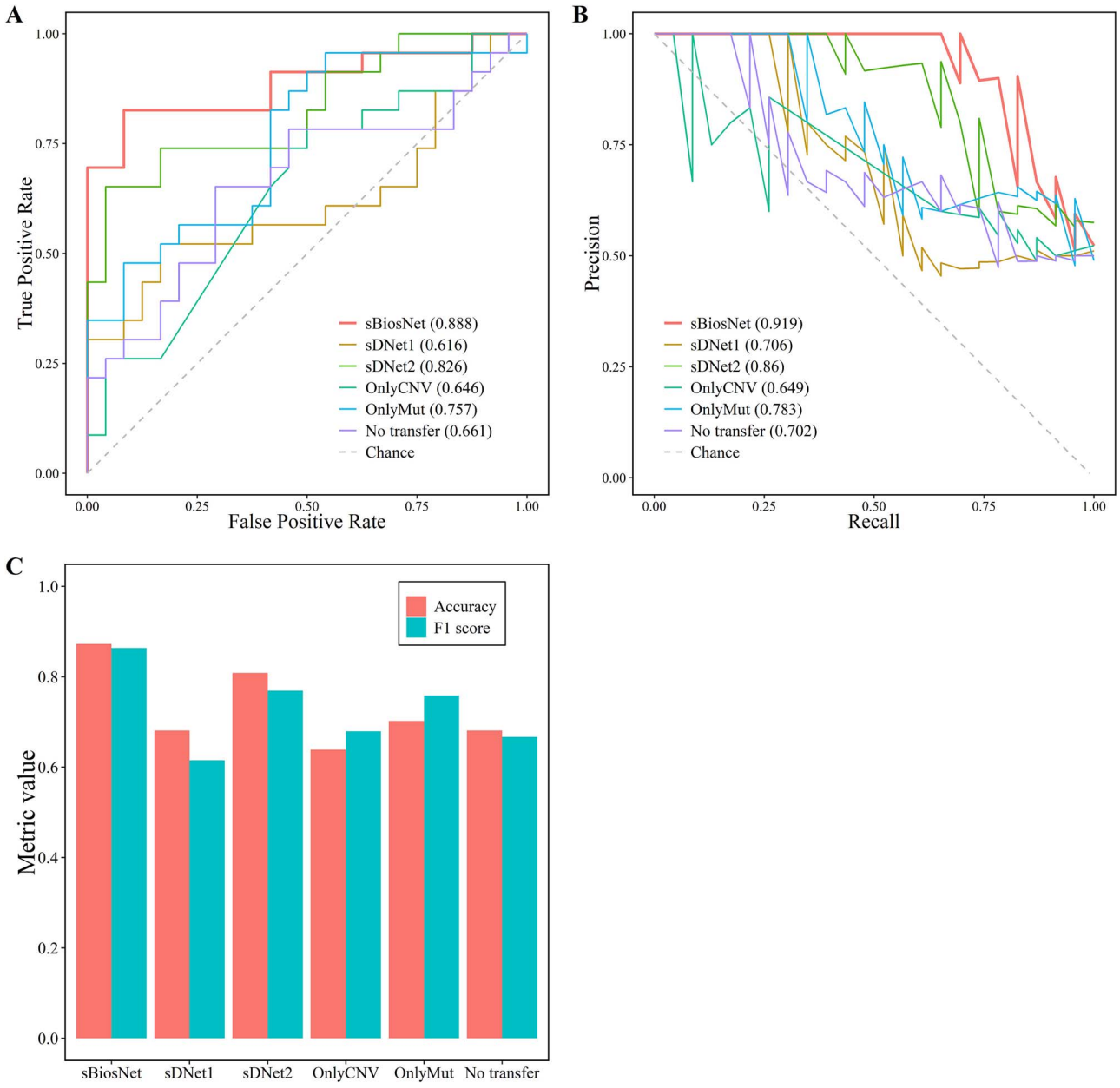

Figure 5. Prediction performance of the sBiosNet in ablation experiments. (A) ROC curves. (B) PR curves. (C) Accuracy and F1 score.

explore their difference between responders and non-responders. The results showed significant differences in gene set feature between two groups, such as PI3K_AKT_MTOR_SIGNALING, NOTCH_SIGNALING, P53_PATHWAY, INFLAMMATORY_RESPONSE, KRAS_SIGNALING_UP and so on (Supplemental Table S17 and Supplemental Table S18). These results showed that, using biological knowledge (such as gene set or pathway), we extracted more complex, higher-level features which reflected patients' biological functions from their genomic mutations or gene expression profiles. This was consistent with the sBiosNet achieving better predictive performance by integrating the biological pathways from the Reactome database.

Identifying the survival of LUAD patients

In clinical practice, we have not only focused on LUAD patients' responses but also their survival outcomes under anti-PD-1 therapy, such as overall survival (OS) and progression-free survival. From the Miao cohort, we identified 21 and 26 patients in the low- and high-risk groups, respectively. In the low-risk group, 23.81% of the patients died while undergoing PD-1 inhibitor treatment, while the high-risk group had a higher mortality rate (42.31%). Meanwhile, we found that LUAD patients in the High-risk group obtained significant shorter OS (11.3 months versus not reached, log-rank $P = .0231$, HR = 3.25, 1.12–9.48, Fig. 7A and Supplemental Table S19) and PFS (1.92 versus 14.70 months, log-rank $P < .0001$, HR = 6.00, 2.77–13.00, Fig. 7B and Supplemental Table S19). We further explore the influence of baseline clinical characters including sex and smoking status using a multivariate COX regression analysis, the results showed the High-risk group patients still faced a high risk of death (HR = 3.35, 1.03–10.92, $P = .0450$) and progress (HR = 6.94, 2.91–16.56, $P < .0001$) (Supplemental Table S19).

There were 15 low-risk LUAD patients were identified from the Frigola cohort, and those patients also had longer OS (not

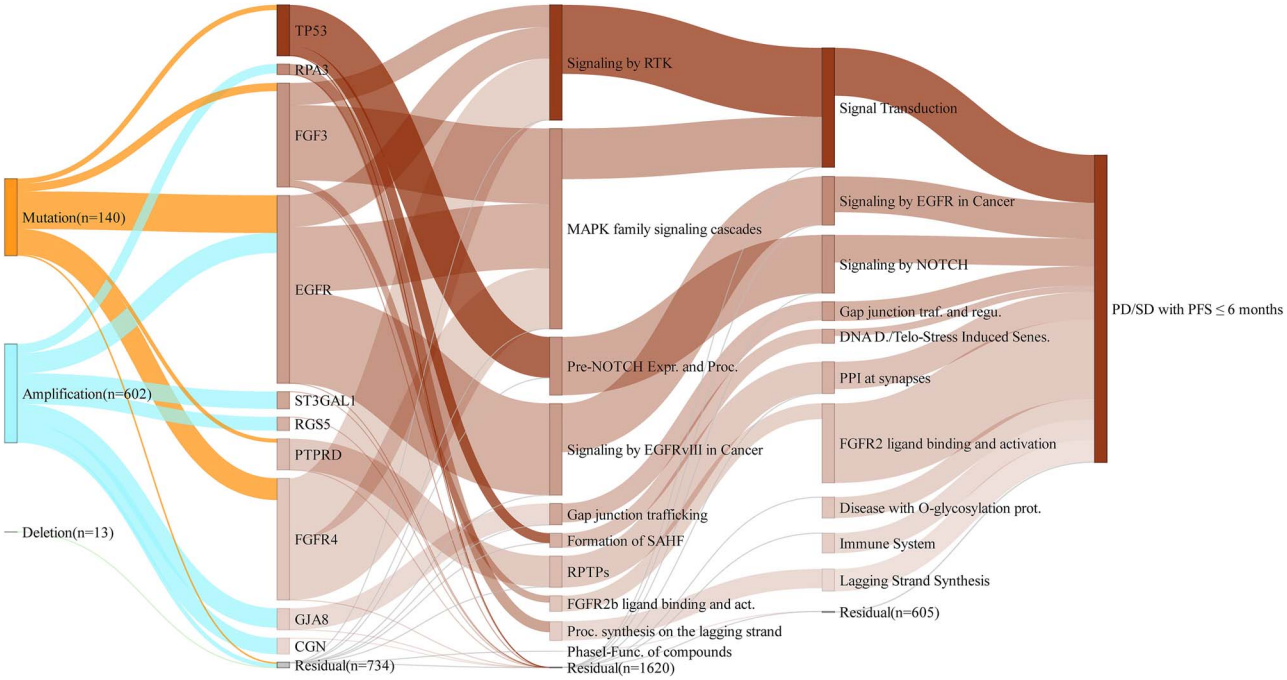

Figure 6. Interpreting the process of the sBiosNet identifies LUAD patients' response to anti-PD-1 therapy. Visualization of the whole sBiosNet shows the relative importance of nodes in each layer. Darker color's nodes are more important, while grey nodes which named 'residual' show the residual importance of the others nodes in each layer. The value in parentheses indicate the total number of nodes included in the category, e.g. there are 734 genes categorized as 'residual'.

reached versus 30.50 months, log-rank $P = .0843$, HR = 2.66, 0.84–8.41, Fig. 7C and Supplemental Table S19) and PFS (30.50 versus 3.53 months, log-rank $P = .0048$, HR = 3.73, 1.41–9.91, Fig. 7D and Supplemental Table S19) than patients in the high-risk group. We also observed the same results through multivariate Cox regression analysis (Supplemental Table S19).

We further identified 152 and 358 patients in the low-risk and high-risk groups from the TCGA cohort, respectively. We compared OS, PFS, disease-free survival (DFS), and disease-specific survival (DSS) between both groups and found that there was no significant difference in OS (4.10 versus 4.11 years, log-rank $P = .9712$, HR = 0.99, 0.72–1.37, Supplemental Fig. S10a), PFS (3.13 versus 2.64 years, log-rank $P = .3546$, HR = 0.87, 0.65–1.17, Supplemental Fig. S10b), DFS (not reached versus 8.08 years, log-rank $P = .7416$, HR = 1.08, 0.68–1.72, Supplemental Fig. S10c), and DSS (not reached versus 6.35 years, log-rank $P = .9032$, HR = 0.98, 0.65–1.47, Supplemental Fig. S10d), suggesting that high-risk patients identified by the sBiosNet were useful only with anti-PD-1 therapy.

Discussion

The sBiosNet, a semi-supervised sparse deep neural network, accurately predicted the LUAD patients' response and survival outcomes under anti-PD-1 therapy by integrating their multi-omics data and the biological relationships between genes and child pathways, and child pathways to parent pathways in the Ractome database, and provided the underlying biological process by which gene mutations and CNVs affected patients' response to anti-PD-1 therapy. Through comparing the predictive performance of the sBiosNet, sDNet1 and models in ablation experiments, we found that biological pathway sparsification contributed the most to the sBiosNet, followed by transfer learning and semi-supervised learning.

Based on biological explanation and the validation results of genes and pathways, we could conclude that gene mutations, copy number variations, and even mRNA expression primarily influenced LUAD patients' response to PD-1 inhibitors at the pathway level. For example, we clearly revealed that TP53 mutation was the most associated with LUAD patients' response to PD-1 inhibitors through NOTCH-associated biological pathways. Hellmann *et al.* [46, 50–52] found that TP53 mutation could increase PD-L1 expression and TMB and affect the NOTCH signaling regulation which could be a predictive biomarker for the response of NSCLC patients to PD-1/PD-L1 inhibitors. And Zhang *et al.* [53, 54] reported that mutations in genes belonging to the NOTCH family could enhance the response to immunotherapy in NSCLC patients and prolong their survival. Meanwhile, we also screened for other biomarkers, such as FGF3, EGFR, and FGFR4 which were associated with EGFR signaling pathway, RTK signaling pathway and MAPK signaling pathway. Akbay *et al.* [55] reported EGFR signaling pathway could remodel the TME to trigger immune escape and mechanistically link treatment response to PD-1 inhibition. The genes FGF3, EGFR, and FGFR4 were also found associated with LUAD patients' response and survival outcome under anti-PD-1 treatment [56–58]. In addition, Shang and Ou *et al.* [59, 60] found that PTPRD mutations influence immunotherapy resistance in cancer patients by affecting the JAK–STAT pathway. All these findings indicate the feasibility of combining the sBiosNet and DeepLIFT algorithms for detecting biomarkers associated with the response of LUAD patients to PD-1 inhibitors and we should also focus more on changes in patient characteristics at the pathway level in subsequent research.

Although the FDA had approved the PD-1 inhibitor, pembrolizumab, in solid tumors with a TMB ≥ 10 mut/Mb [61], concerns exist whether TMB thresholds for predicting response to PD-1 blockade are equivalent across the spectrum of solid tumors. We therefore combined TMB and logistic regression to demonstrate that the predictive performance of TMB as a biomarker of response to PD-1 inhibitors in LUAD patients. As the results from SGE202417 and GSE111414, the contribution of

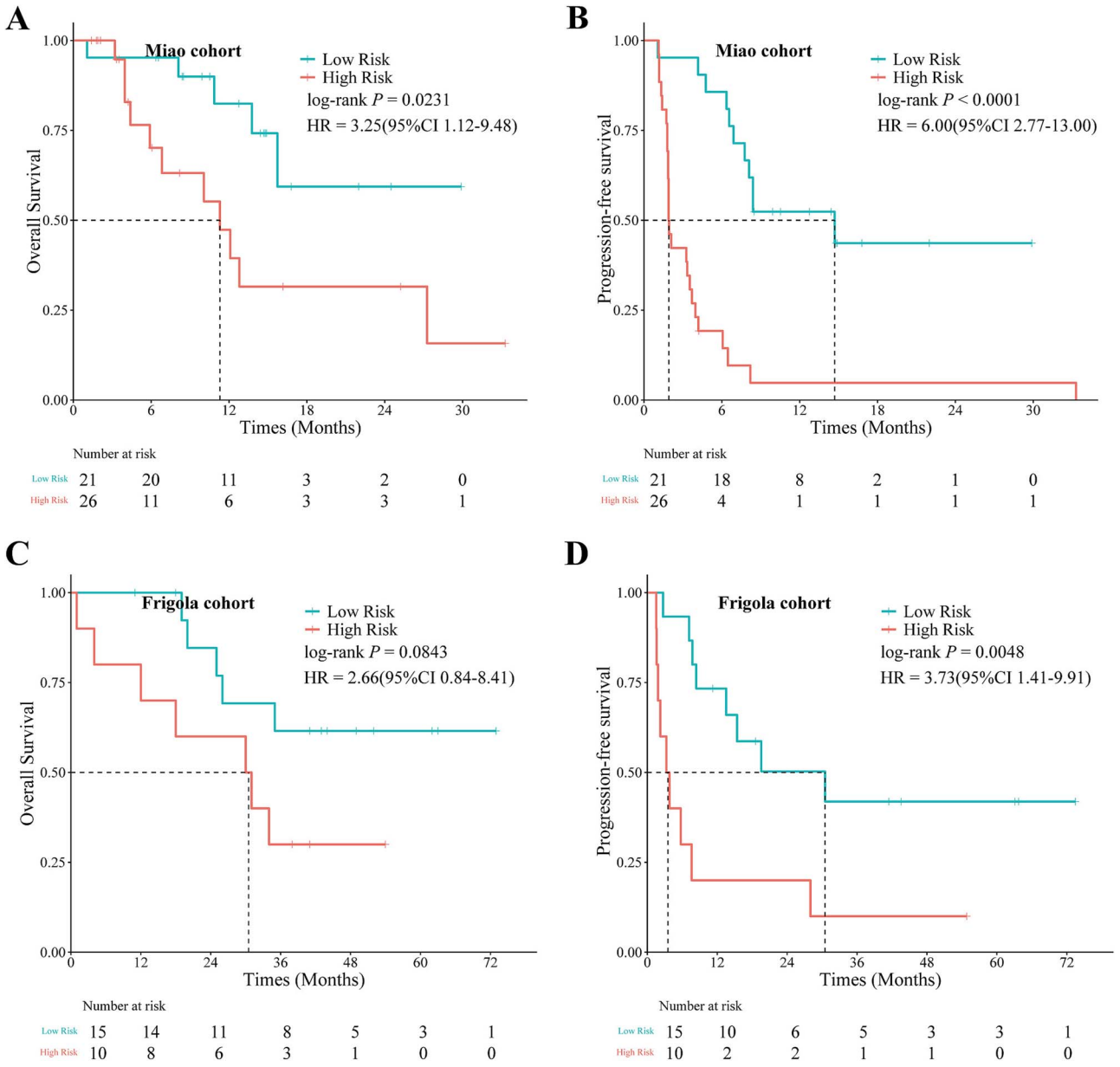

Figure 7. Kaplan–Meier estimates of LUAD patients between high-risk group and low-risk group. Kaplan–Meier curves of (A) OS and (B) PFS for LUAD patients undergoing anti-PD-1 therapy in Miao cohort. (C) OS and (d) PFS for LUAD patients undergoing anti-PD-1 therapy in Frigola cohort.

individual gene to identify the response of LUAD patients to PD-1 inhibitors was very small. Therefore, traditional machine learning models such as RF and SVM were unable to learn biological features related to the response of LUAD patients to PD-1 from genomic mutation and CNV profiles. We suggested this was one of the reasons that Logistic + TMB had better performance than RF and SVM. Currently, there were multiple different methods to calculate TMB, but the optimal approach was based on exome-wide sequencing analysis encompassing ~30 Mb [62], which was consistent with our study. There were also some factors impacted the TMB score, including the amount of genome interrogated, filtering of alterations, tumor heterogeneity, and read depth [63–65], we would further explore the effects of these factors in subsequent studies.

Our study also has some limitations. First, the sample sizes of all the Rizvi, Miao, and Frigola cohorts were relatively small. We will further explore the properties of sBiosNet by using larger cohorts. Second, the sBiosNet's performance may vary with immunotherapy combinations, such as combination of PD-1 and chemotherapy. Third, there were also some potential confounding factors, such as co-mutations, TME heterogeneity that may affect the sBiosNet's performance. In addition, researchers need to reconstruct the network structure and retrain sBiosNet when using different cohorts when predicting responses in other tumor patients.

In conclusion, sBiosNet not only accurately identifies the response and survival of LUAD patients under anti-PD-1 therapy to reduce unnecessary treatment in non-responders but also reveals relevant biological processes and provides clear and rational interpretations.

Sanctions

None of the authors are included in any list related to trade sanctions, nor are they employed by any organization or entity on any list related to trade sanctions. Our article do not

contain military or defense-related or other regulated technical information.

Key Points

- sBiosNet accurately identifies lung adenocarcinoma (LUAD) patients' response to progressive disease (PD)–1 inhibitors.
- sBiosNet identifies the survival of LUAD patients treated with PD-1 inhibitors.
- sBiosNet reveals complex biological processes of resistance for PD-1 inhibitors.

Author contributions

Conceptualization: W-YY, Z-LC, LK, CL. Data curation: W-YY, Z-LC, W-YR. Software and Visualization: Z-LC and W-YY. Writing – original draft: W-YY and Z-LC. Validation and Writing – review & editing: CL, X-HY, W-LY, W-YR, LS, HJ, WM, ZX and W-HS. All authors have read and approved the final manuscript. All authors have read and approved the final manuscript.

Supplementary data

Supplementary data are available at *Briefings in Bioinformatics* online.

Conflict of interest: The authors declare that they have no conflict of interest.

Funding

This study was supported by the National Natural Science Foundation of China (project numbers: 82304250, 82273734, and 82003551).

Data availability

The dataset of the Rizvi cohort is available from the CBioPortal for Cancer Genomics: MSK-IMPACT clinical sequencing cohort for non-small cell cancer (MSK, JCO 2018). http://www.cbioportal.org/study?id=nsclc_pd1_msk_2018. The clinical information and multi-omics data of the Miao cohort were downloaded from the supplementary tables at https://www.nature.com/articles/s41588-018-0200-2#Sec24. The clinical information and multi-omics data of the Frigola cohort is obtained from https://febs.onlinelibrary.wiley.com/doi/10.1002/1878-0261.12891. TCGA dataset was downloaded from the UCSC XENA database. The relationship of gene-to-child pathways and child-to-parent pathways in the Reactome database was downloaded at https://reactome.org/download-data. The dataset of the Hellmann cohort is downloaded from https://www.cell.com/cancer-cell/fulltext/S1535-6108(18)30123-5. The data used and/or analyzed during the current study are available from the corresponding author upon reasonable request.

Ethics approval

Not applicable

References

1. Markham A. Atezolizumab: First global approval. *Drugs* 2016;**76**:1227–32. https://doi.org/10.1007/s40265-016-0618-8
2. Hodi FS, O'day SJ, DF MD. *et al.* Improved survival with ipilimumab in patients with metastatic melanoma. *N Engl J Med* 2010;**363**:711–23. https://doi.org/10.1056/NEJMoa1003466
3. Damhofer H, Helin K. EZH2i unlocks PDAC immune surveillance. *Nat Cancer* 2023;**4**:781–3. https://doi.org/10.1038/s43018-023-00562-7
4. Sensi B, Angelico R, Toti L. *et al.* Mechanism, potential, and concerns of immunotherapy for hepatocellular carcinoma and liver transplantation, Curr. *Mol Pharmacol* 2024;**17**:e18761429310703.
5. Lim DV, Woo WH, Lim JX. *et al.* Targeting mutant-p53 for cancer treatment: Are we there yet? *Curr Mol Pharmacol* 2024;**17**:e140923221042.
6. Manohar SM. At the crossroads of TNF α signaling and cancer. *Curr Mol Pharmacol* 2024;**17**:e060923220758.
7. Liu L, Xie Y, Yang H. *et al.* HPVTIMER: A shiny web application for tumor immune estimation in human papillomavirus-associated cancers. *Imeta* 2023;**2**:e130.
8. Lin A, Jiang A, Huang L. *et al.* From chaos to order: Optimizing fecal microbiota transplantation for enhanced immune checkpoint inhibitors efficacy. *Gut Microbes* 2025;**17**:2452277.
9. Peng S, Lin A, Jiang A. *et al.* CTLs heterogeneity and plasticity: Implications for cancer immunotherapy. *Mol Cancer* 2024;**23**:58.
10. Taube JM, Klein A, Brahmer JR. *et al.* Association of PD-1, PD-1 ligands, and other features of the tumor immune microenvironment with response to anti–PD-1 therapy. *Clin Cancer Res* 2014;**20**:5064–74. https://doi.org/10.1158/1078-0432.CCR-13-3271
11. Restifo NP, Smyth MJ, Snyder A. Acquired resistance to immunotherapy and future challenges. *Nat Rev Cancer* 2016;**16**:121–6. https://doi.org/10.1038/nrc.2016.2
12. Tanaka T, Yoshida T, Masuda K. *et al.* Prognostic role of modified Glasgow prognostic score in elderly non-small cell lung cancer patients treated with anti-PD-1 antibodies. *Respir Investig* 2023;**61**:74–81. https://doi.org/10.1016/j.resinv.2022.10.003
13. Gandhi L, Rodríguez-Abreu D, Gadgeel S. *et al.* Pembrolizumab plus chemotherapy in metastatic non–small-cell lung cancer. *N Engl J Med* 2018;**378**:2078–92. https://doi.org/10.1056/NEJMoa1801005
14. Wu Y-L, Lu S, Cheng Y. *et al.* Nivolumab versus docetaxel in a predominantly Chinese patient population with previously treated advanced NSCLC: CheckMate 078 randomized phase III clinical trial. *J Thorac Oncol* 2019;**14**:867–75. https://doi.org/10.1016/j.jtho.2019.01.006
15. Hamid O, Robert C, Daud A. *et al.* Five-year survival outcomes for patients with advanced melanoma treated with pembrolizumab in KEYNOTE-001. *Ann Oncol* 2019;**30**:582–8. https://doi.org/10.1093/annonc/mdz011
16. Hegde PS, Chen DS. Top 10 challenges in cancer immunotherapy. *Immunity* 2020;**52**:17–35. https://doi.org/10.1016/j.immuni.2019.12.011
17. Feng Y, Wang Y, Guo K. *et al.* The value of WNT5A as prognostic and immunological biomarker in pan-cancer. *Ann Transl Med* 2022;**10**:466.
18. Topalian SL, Taube JM, Anders RA. *et al.* Mechanism-driven biomarkers to guide immune checkpoint blockade in cancer therapy. *Nat Rev Cancer* 2016;**16**:275–87. https://doi.org/10.1038/nrc.2016.36
19. Patel SP, Kurzrock R. PD-L1 expression as a predictive biomarker in cancer immunotherapy. *Mol Cancer Ther* 2015;**14**:847–56. https://doi.org/10.1158/1535-7163.MCT-14-0983
20. Bai X, Wu D-H, Ma S-C. *et al.* Development and validation of a genomic mutation signature to predict response to PD-1 inhibitors in non-squamous NSCLC: A multicohort study. *J Immunother Cancer* 2020;**8**:e000381.

21. Jardim DL, Goodman A, de Melo Gagliato D. *et al.* The challenges of tumor mutational burden as an immunotherapy biomarker. *Cancer Cell* 2021;**39**:154–73. https://doi.org/10.1016/j.ccell.2020.10.001
22. Subbiah V, Solit D, Chan T. *et al.* The FDA approval of pembrolizumab for adult and pediatric patients with tumor mutational burden (TMB)≥ 10: A decision centered on empowering patients and their physicians. *Ann Oncol* 2020;**31**:1115–8. https://doi.org/10.1016/j.annonc.2020.07.002
23. Strickler JH, Hanks BA, Khasraw M. Tumor mutational burden as a predictor of immunotherapy response: Is more always better? *Clin Cancer Res* 2021;**27**:1236–41. https://doi.org/10.1158/1078-0432.CCR-20-3054
24. Riaz N, Havel JJ, Kendall SM. *et al.* Recurrent SERPINB3 and SERPINB4 mutations in patients who respond to anti-CTLA4 immunotherapy. *Nat Genet* 2016;**48**:1327–9. https://doi.org/10.1038/ng.3677
25. Johnson DB, Lovly CM, Flavin M. *et al.* Impact of NRAS mutations for patients with advanced melanoma treated with immune therapies. *Cancer Immunol Res* 2015;**3**:288–95. https://doi.org/10.1158/2326-6066.CIR-14-0207
26. Gao J, Shi LZ, Zhao H. *et al.* Loss of IFN-γ pathway genes in tumor cells as a mechanism of resistance to anti-CTLA-4 therapy. *Cell* 2016;**167**:397–404.e399.
27. Kato S, Goodman A, Walavalkar V. *et al.* Hyperprogressors after immunotherapy: Analysis of genomic alterations associated with accelerated growth rate. *Clin Cancer Res* 2017;**23**:4242–50. https://doi.org/10.1158/1078-0432.CCR-16-3133
28. Zhang L, Cao L, Li S. *et al.* Biologically interpretable deep learning to predict response to immunotherapy in advanced melanoma using mutations and copy number variations. *J Immunother* 2023;**46**:221–31. https://doi.org/10.1097/CJI.0000000000000475
29. Gillespie M, Jassal B, Stephan R. *et al.* The reactome pathway knowledgebase 2022. *Nucleic Acids Res* 2022;**50**:D687–92. https://doi.org/10.1093/nar/gkab1028
30. Cheng DT, Mitchell TN, Zehir A. *et al.* Memorial Sloan Kettering-integrated mutation profiling of actionable cancer targets (MSK-IMPACT): A hybridization capture-based next-generation sequencing clinical assay for solid tumor molecular oncology. *J Mol Diagn* 2015;**17**:251–64. https://doi.org/10.1016/j.jmoldx.2014.12.006
31. Eisenhauer EA, Therasse P, Bogaerts J. *et al.* New response evaluation criteria in solid tumours: Revised RECIST guideline (version 1.1). *Eur J Cancer* 2009;**45**:228–47. https://doi.org/10.1016/j.ejca.2008.10.026
32. Rizvi H, Sanchez-Vega F, La K. *et al.* Molecular determinants of response to anti–programmed cell death (PD)-1 and anti–programmed death-ligand 1 (PD-L1) blockade in patients with non–small-cell lung cancer profiled with targeted next-generation sequencing. *J Clin Oncol* 2018;**36**:633.
33. George S, Miao D, Demetri GD. *et al.* Loss of PTEN is associated with resistance to anti-PD-1 checkpoint blockade therapy in metastatic uterine leiomyosarcoma. *Immunity* 2017;**46**:197–204. https://doi.org/10.1016/j.immuni.2017.02.001
34. Miao D, Margolis CA, Vokes NI. *et al.* Genomic correlates of response to immune checkpoint blockade in microsatellite-stable solid tumors. *Nat Genet* 2018;**50**:1271–81. https://doi.org/10.1038/s41588-018-0200-2
35. Frigola J, Navarro A, Carbonell C. *et al.* Molecular profiling of long-term responders to immune checkpoint inhibitors in advanced non-small cell lung cancer. *Mol Oncol* 2021;**15**:887–900. https://doi.org/10.1002/1878-0261.12891
36. Ramos AH, Lichtenstein L, Gupta M. *et al.* Oncotator: Cancer variant annotation tool. *Hum Mutat* 2015;**36**:E2423–9. https://doi.org/10.1002/humu.22771
37. Bro R, Smilde AK. Principal component analysis. *Anal Methods* 2014;**6**:2812–31.
38. Van der Maaten L, Hinton G. Visualizing data using t-SNE. *J Mach Learn Res* 2008;**9**:2579–605.
39. McInnes L, Healy J, Melville J. Umap: Uniform manifold approximation and projection for dimension reduction. *J Open Source Softw* 2018;**3**:861.
40. Roh W, Chen P-L, Reuben A. *et al.* Integrated molecular analysis of tumor biopsies on sequential CTLA-4 and PD-1 blockade reveals markers of response and resistance. *Sci Transl Med* 2017;**9**:eaah3560.
41. Hinton G, Vinyals O, Dean J. Distilling the knowledge in a neural network. *Computer Science* 2015;**14**:38–9.
42. Guo C, Pleiss G, Sun Y. *et al.* On calibration of modern neural networks. *34th International Conference on Machine Learning*, Sydney, Australia, PMLR, 2017;**3–8**:1321–30.
43. Lee D-H. Pseudo-label: The simple and efficient semi-supervised learning method for deep neural networks. *Workshop on Challenges in Representation Learning, Atlanta, ICML*, 2013;**3**:896.
44. Zhang H, Cisse M, Dauphin YN. *et al.* Mixup: Beyond empirical risk minimization, arXiv preprint arXiv:1710.09412. 2017.
45. Shrikumar A, Greenside P, Kundaje A. Learning important features through propagating activation differences. *International Conference on Machine Learning*, PMLR, 2017, 3145–53.
46. Hellmann MD, Nathanson T, Rizvi H. *et al.* Genomic features of response to combination immunotherapy in patients with advanced non-small-cell lung cancer. *Cancer Cell* 2018;**33**:843–852.e844.
47. Trefny MP, Rothschild SI, Uhlenbrock F. *et al.* A variant of a killer cell immunoglobulin-like receptor is associated with resistance to PD-1 blockade in lung cancer. *Clin Cancer Res* 2019;**25**:3026–34. https://doi.org/10.1158/1078-0432.CCR-18-3041
48. Subramanian A, Tamayo P, Mootha VK. *et al.* Gene set enrichment analysis: A knowledge-based approach for interpreting genome-wide expression profiles. *Proc Natl Acad Sci* 2005;**102**:15545–50.
49. Mootha VK, Lindgren CM, Eriksson K-F. *et al.* PGC-1α-responsive genes involved in oxidative phosphorylation are coordinately downregulated in human diabetes. *Nat Genet* 2003;**34**:267–73.
50. Dong Z-Y, Zhong W-Z, Zhang X-C. *et al.* Potential predictive value of TP53 and KRAS mutation status for response to PD-1 blockade immunotherapy in lung adenocarcinoma. *Clin Cancer Res* 2017;**23**:3012–24. https://doi.org/10.1158/1078-0432.CCR-16-2554
51. Li H, Yang L, Wang Y. *et al.* Integrative analysis of TP53 mutations in lung adenocarcinoma for immunotherapies and prognosis. *BMC Bioinformatics* 2023;**24**:155.
52. Shi Q, Xue C, Zeng Y. *et al.* Notch signaling pathway in cancer: From mechanistic insights to targeted therapies. *Signal Transduct Target Ther* 2024;**9**:128.
53. Zhang K, Hong X, Song Z. *et al.* Identification of deleterious NOTCH mutation as novel predictor to efficacious immunotherapy in NSCLC. *Clin Cancer Res* 2020;**26**:3649–61. https://doi.org/10.1158/1078-0432.CCR-19-3976
54. Long J, Wang D, Yang X. *et al.* Identification of NOTCH4 mutation as a response biomarker for immune checkpoint inhibitor therapy. *BMC Med* 2021;**19**:1–14.

55. Akbay EA, Koyama S, Carretero J. *et al.* Activation of the PD-1 pathway contributes to immune escape in EGFR-driven lung tumors. *Cancer Discov* 2013;**3**:1355–63. https://doi.org/10.1158/2159-8290.CD-13-0310
56. Dou S, Zhang L, Wang C. *et al.* EGFR mutation and 11q13 amplification are potential predictive biomarkers for immunotherapy in head and neck squamous cell carcinoma. *Front Immunol* 2022;**13**:813732.
57. Gainor JF, Shaw AT, Sequist LV. *et al.* EGFR mutations and ALK rearrangements are associated with low response rates to PD-1 pathway blockade in non-small cell lung cancer: A retrospective analysis. *Clin Cancer Res* 2016;**22**:4585–93. https://doi.org/10.1158/1078-0432.CCR-15-3101
58. Yi C, Chen L, Lin Z. *et al.* Lenvatinib targets FGF receptor 4 to enhance antitumor immune response of anti–programmed cell Death-1 in HCC. *Hepatology* 2021;**74**:2544–60. https://doi.org/10.1002/hep.31921
59. Shang X, Zhang W, Zhang X. *et al.* PTPRD/PTPRT mutation as a predictive biomarker of immune checkpoint inhibitors across multiple cancer types. *Front Immunol* 2022;**13**:991091.
60. Ou C, Peng Q, Zeng C. An integrative prognostic and immune analysis of PTPRD in cancer. *Math Biosci Eng* 2022;**19**:5361–79. https://doi.org/10.3934/mbe.2022251
61. Marcus L, Fashoyin-Aje LA, Donoghue M. *et al.* FDA approval summary: Pembrolizumab for the treatment of tumor mutational burden-high solid tumors. *Clin Cancer Res* 2021;**27**:4685–9. https://doi.org/10.1158/1078-0432.CCR-21-0327
62. Kim H, Zheng S, Amini SS. *et al.* Whole-genome and multisector exome sequencing of primary and post-treatment glioblastoma reveals patterns of tumor evolution. *Genome Res* 2015;**25**:316–27. https://doi.org/10.1101/gr.180612.114
63. Garofalo A, Sholl L, Reardon B. *et al.* The impact of tumor profiling approaches and genomic data strategies for cancer precision medicine. *Genome Med* 2016;**8**:79.
64. Budczies J, Allgäuer M, Litchfield K. *et al.* Optimizing panel-based tumor mutational burden (TMB) measurement. *Ann Oncol* 2019;**30**:1496–506. https://doi.org/10.1093/annonc/mdz205
65. Budczies J, Kazdal D, Allgäuer M. *et al.* Quantifying potential confounders of panel-based tumor mutational burden (TMB) measurement. *Lung Cancer* 2020;**142**:114–9. https://doi.org/10.1016/j.lungcan.2020.01.019

Briefings in Bioinformatics, 2025, **26(5)**, bbaf479
https://doi.org/10.1093/bib/bbaf479
Case Study